Tailoring optical properties of WO_3 films in the visible to infrared range by ion bombardment and its description by an oscillator model

Matthias Merz, Johannes Eisenmenger, Bernd Heinz, and Paul Ziemann*
Abteilung Festkörperphysik, Universität Ulm, D-89069 Ulm, Germany
(Received 28 January 2002; revised manuscript received 19 April 2002; published 13 November 2002)

Evaporated and sputtered tungstentrioxide (WO_3) films were bombarded with 300-keV He^+ and Ar^+ ions, respectively, and the resulting changes of the real $[n(\lambda)]$ and imaginary $[k(\lambda)]$ parts of the refractive index in the visible to infrared range of the wavelength λ were determined *in situ*. The primary effect of an ion-induced blue coloration is directly reflected by an absorption band centered at 1100 nm, which is growing for increasing ion fluences and exponentially approaching saturation. This monotonous increase of absorption is accompanied by changes of $n(\lambda)$ with a characteristic fixed point $n(\lambda^*)$ independent of the ion bombardment, while for $\lambda > \lambda^*$ an ion-induced increase and for $\lambda < \lambda^*$ a decrease of n are observed as compared to the unbombarded as-prepared samples. The experimental results can be quantitatively explained by assuming a superposition of a standard Cauchy dispersion representing the unbombarded WO_3 matrix and ion-induced Lorentz oscillators. While the density of these oscillators as well as their damping coefficients exhibit an exponential saturation behavior for increasing ion fluences, their eigenfrequencies as well as the matrix contribution are practically independent of the bombardment.

DOI: 10.1103/PhysRevB.66.184102 PACS number(s): 61.66.Fn, 61.80.Jh, 61.82.Ms, 78.20.Ci

I. INTRODUCTION

Due to its property of being chromogenic, tungstentrioxide (WO_3) has attracted much interest during the last decade. Among the various techniques to change the optical properties of WO_3, electrochemical intercalation of light ions such as Li^+ or H^+ appears especially popular, since in this way the visible color as well as the absorption behavior in the infrared can be reversibly switched and controlled by applying appropriate voltages. In the visible, this electrochromic effect transforms stoichiometric WO_3 from a transparent state into a deep blue color, which can be macroscopically attributed to an absorption band centered at approximately 1000 nm.[1] Microscopically, it is widely accepted that color centers of the type $H_x W_x^{+V} W_{1-x}^{+VI} O_3$ are formed with tungsten atoms in a reduced state of oxidation number $+V$. The absorption process is then interpreted by the formation of a small polaron[2] and its transfer by hopping between neighboring W^{+V} and W^{+VI} sites. The details of the various electrochromic properties of WO_3 can be found in reviews.[3,4]

Alternatively, WO_3 can be colored by exposing it to UV light resulting in practically the same absorption band as described above for intercalation.[5] This photochromic effect, however, exhibits a threshold behavior[6] in that the light energy has to exceed 3.3 eV, i.e., the electronic gap of amorphous WO_3 of 3.25 eV (Refs. 7 and 5) pointing to electron-hole pairs as one necessary ingredient for UV coloration. Another one seems to be H_2O,[8,9] which almost inevitably is incorporated into WO_3 films during their preparation. This built-in water can act as an internal reservoir providing, after dissociation, H^+ ions resulting in the same color centers as in the electrochromic case. Still another route towards coloration is based on the creation of oxygen vacancies, each resulting in two reduced W^{+V} atoms. As a consequence, substoichiometric films show a light blue color. One way to create such vacancies and, thus, to color WO_3 samples, is by heating above 150 °C, naturally termed a thermochromic effect.[8] Alternatively, oxygen vacancies are also obtained by corresponding displacements during the bombardment with ions triggered by collisions between the projectiles and target atoms. As an example, by applying low-energy Ar^+-ion bombardment, Dixon *et al.* could show[10] that W^{+VI} states are transformed into W^{+V} and W^{+IV} states due to the ion-induced removal of surface oxygen atoms.

Since the bombardment of differently prepared WO_3 films with ions at medium energies of typically some hundred keV is in the center of the present work, related previous results will be shortly summarized in the following. Among the first properties of WO_3 films studied after ion irradiation was their density. Here, it is important to note that evaporated WO_3 samples exhibit a very ''open'' morphology with strongly reduced average densities. It turns out that these more open structured, evaporated films show much more pronounced photo- or thermochromic effects than, e.g., sputtered WO_3 films, which practically have the bulk WO_3 density of 7.16 g/cm^3.[3] Thus, when bombarding evaporated as opposed to sputtered WO_3 films with energetic ions, one has to take into account a possible densification. Such an effect has been reported for different projectiles as well as energies.[11,12] This densification is especially important when discussing ion-induced changes of the optical properties such as the refractive index, which are in the focus of the present work.

Another property of importance is the electrical conductivity σ of WO_3 films. In their stoichiometric state they are insulators at ambient temperature due to the large gap value given above. If colored, however, by any of the above three chromogenic effects, the change of the optical behavior is accompanied by an increase of the electrical conductivity over many orders of magnitude with a temperature dependence exhibiting Mott's law $\ln \sigma \propto T^{-1/4}$ indicating a ''vari-

able range hopping'' conductivity.[13] The issue of conductivity changes induced by ion bombardment of WO_3 films has been adressed by Miyakawa *et al.*[14] In contrast to the present work, however, the He^+, Ar^+, and W^+ ions were implanted, i.e., they came to rest within the WO_3 films. In the present case, the energy of the projectiles is adjusted to guarantee that they penetrate the WO_3 film thereby transferring energy to the sample via electronic and nuclear loss mechanisms, and are implanted into the underlying substrate. Such irradiation as opposed to implantation experiments on evaporated and sputtered WO_3 films were reported recently by our group[15] with emphasis on changes of the hopping conductivity induced by ion bombardment at different temperatures. In the present work we focus on the spectral behavior of ion-induced changes of the real $[n(\lambda)]$ and imaginary $[k(\lambda)]$ parts of the complex refractive index $\tilde{n}=n+ik$ within the wavelength range 400 nm$\leqslant\lambda\leqslant$1600 nm.

II. EXPERIMENT

As mentioned already above, the morphology and, related to that, the density of WO_3 films strongly depend on the method used for their preparation with evaporated samples exhibiting a more open structure with a significantly reduced average density as compared to sputtered films. To check for possible influences of these structural differences on the results of ion bombardment experiments, in the present study three different techniques were applied to prepare WO_3 films: (i) Thermal evaporation from Mo boats within a commercial high-vacuum recipient, (ii) electron-beam evaporation within an ultrahigh-vacuum system, and (iii) reactive rf magnetron sputtering. In case (i), ingots from pressed WO_3 powder were evaporated from directly heated Mo boats at a typical rate of 0.3 nm/s and a pressure during evaporation of 10^{-5} mbar. In case (ii), pieces of a commercial WO_3 sputter target (purity 99.99%) were evaporated within an UHV recipient of a base pressure of 5×10^{-9} mbar at a rate of 0.5 nm/s. In case of the rf magnetron sputtering a reactive oxygen/argon mixture was used ($Ar:O_2=3:1$) at a total pressure of 9×10^{-3} mbar. Controlling and keeping the sputtering power fixed at 70 W resulted in typical deposition rates of 0.02 nm/s. In all cases the samples were deposited onto glass (BK7) substrates held at nominally ambient temperature or slightly below; their thickness D ranged between 55 nm and 150 nm. These WO_3 films all appeared optically transparent in the as-prepared state indicating that they were at or close to the desired stoichiometry. This conclusion could be independently corroborated by Rutherford backscattering (RBS) experiments using 700-keV He^{2+} ions. Independent of the preparation procedure all samples were x-ray amorphous as revealed by x-ray diffraction.

To ion bombard the WO_3 films, they were mounted onto a movable sample holder within a UHV chamber connected via a differentially pumped additional smaller chamber to the high-voltage beamline of an ion implantor (maximum acceleration voltage 350 kV) providing the 300-keV Ar^+ and He^+ ions used in this study. Important quantities characterizing an ion bombardment experiment are the projected ranges as well as the damage profiles of the ions. Both can be calculated by Monte Carlo simulation programs such as SRIM2000,[16] delivering also the parameters of the mean projected range R_p and its longitudinal straggling ΔR_p as well as the nuclear, $\langle(dE/dx)_n\rangle$, and electronic, $\langle(dE/dx)_e\rangle$, energy loss of the projectiles averaged over the bombarded film thickness. In the present study emphasis is put on the effect of ion-induced defects on the WO_3 properties rather than of implanted species. Thus, the energy of the projectiles is adjusted to guarantee that the corresponding projected ranges are significantly larger than the film thickness. If the condition $R_p-\Delta R_p>D$ holds, the concentration of implanted projectiles can be neglected. In the present case of 300-keV He^+ and Ar^+, the values are $R_p(He^+)=1200$ nm, $\Delta R_p(He^+)=240$ nm, and $R_p(Ar^+)=215$ nm, $\Delta R_p(Ar^+)=106$ nm assuming a density of 7.04 g/cm^3 for the sputtered WO_3 films as determined by combined optical and RBS measurements. Thus, for a typical film thickness of 100 nm even for the heavier projectiles and high fluences (10^{15} cm^{-2}) the average concentration of implanted species is well below 0.1%. Further details on the ion bombardment conditions and sample arrangements as well as on the resulting damage profiles as calculated by SRIM can be found in Ref. 15.

The experimental setup allows an *in situ* determination of the complex refractive index, i.e., after each irradiation step the real and imaginary parts, $n(\lambda)$ and $k(\lambda)$, are obtained by measuring transmittance and reflectance spectra, respectively, under the condition of normal incidence. All spectra are normalized to the incoming intensity thereby excluding the influence of fluctuating intensities of the light source (100-W halogen lamp). A monochromator allowed to select wavelengths in the range 400 nm $\leqslant\lambda\leqslant$1600 nm with a spectral resolution of $\Delta\lambda=9$ nm. A schematic overview of the optical detection system is given in Ref. 11.

For the determination of the complex index of refraction from the transmittance and reflectance spectra a model is needed describing the optical properties of the combined film/substrate system. For this purpose, a homogeneous isotropic thin layer is considered bounded by parallel planar surfaces and supported by a substrate of finite thickness. Multiple incoherently summed reflections from the substrate interfaces and coherent superposition of the amplitudes within the film are taken into account. For the reflectance measurements, normal incidence is assumed neglecting a 2° deviation. The effect of this simplification, as well as that of the assumption of a homogeneous layer, are discussed in detail in Ref. 17. With $n(\lambda)$ and $k(\lambda)$ known for the substrate, the corresponding values for the film can be determined numerically using Fresnel coefficients for the transmission and reflection at the interfaces and adjusting the film thickness as to avoid unphysical multiple valued solutions for n and k.[11] The applied numerical procedures as well as the underlying formulas are described in Refs. 18 and 19.

III. RESULTS AND DISCUSSION

As a first application of the above numerical recipe to extract the complex index of refraction, in Fig. 1 the real part $n(\lambda)$ is plotted for the as-prepared sputtered or evaporated

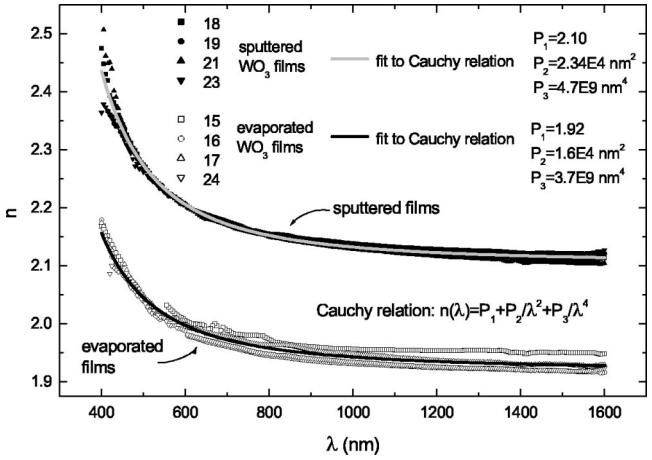

FIG. 1. Dispersion of the real part of the refractive index $n(\lambda)$ for various sputtered (closed symbols) and evaporated (open symbols) WO_3 films. The samples are specified by the number attached to each symbol. The solid lines represent the corresponding standard Cauchy dispersions obtained by least-squares fitting to the data with parameters given in the inset.

WO_3 films. Additionally to the experimental results, fits to the Cauchy relation

$$n(\lambda) = P_1 + P_2/\lambda^2 + P_3/\lambda^4 \tag{1}$$

describing the standard dispersion are added as solid lines. Clearly, the sputtered films (closed symbols) exhibit an offset by approximately 10% towards higher n values reflecting the correspondingly higher density of these samples as compared to the evaporated ones (open symbols).

This density difference can be completely removed by ion bombarding evaporated WO_3 films with heavy ions such as Ar^+ while for light He^+ ions the induced density changes are practically negligible.[11] Closer inspection of Fig. 1 also reveals a larger spread of n values from sample to sample for evaporated films. This reflects the tendency to obtain slightly understoichiometric WO_3 films by evaporation since, during heating, oxygen starts to diffuse out of the WO_3 used to evaporate. This effect manifests itself even more clearly in the imaginary part $k(\lambda)$, which is practically constant within the above range of wavelengths with k values between 0.005 and 0.01 indicating optical transparency for sputtered films, while some evaporated films already exhibit a broad absorption band centered at about 1000 nm with k values up to 0.03 signaling the onset of coloration due to oxygen vacancies.

Next, the effect of 300-keV Ar^+-ion bombardment on the refractive index of evaporated WO_3 films will be described. For that purpose, in Fig. 2(a) the real part n and in Fig. 2(b) the imaginary part k are presented as a function of the wavelength for a series of irradiation steps on one and the same sample (number 15, cf. Fig. 1) with fluences as given in the inset. There are two prominent features evident in Fig. 2, the most notable being the strong increase of the imaginary part $k(\lambda)$ exhibiting a broad absorption band centered at about 1100 nm, reflecting the ion-induced blue coloration of the WO_3 film. This is in agreement with what is known for electrochemically colored samples, for which absorption bands

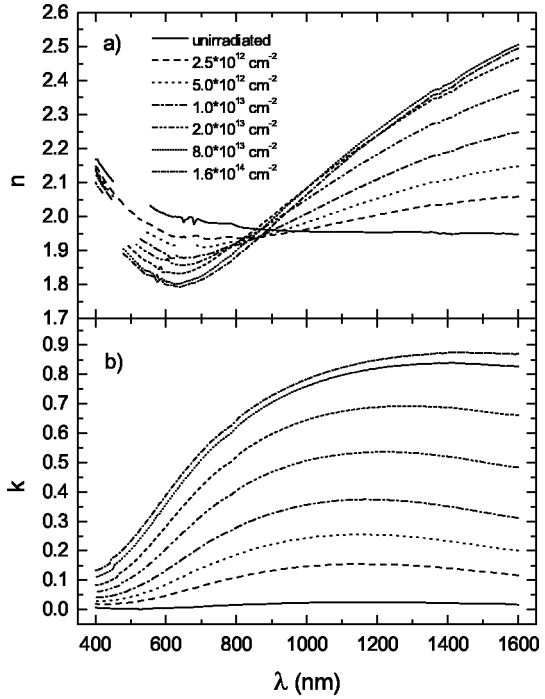

FIG. 2. Dispersion of (a) the real part $n(\lambda)$ and of (b) the imaginary part $k(\lambda)$ for an evaporated WO_3 film (number 15) as changed by 300-keV Ar^+-ion bombardment with fluences given in the inset (missing data points for small λ are due to experimental problems when changing the filter of the monochromator).

centered between 1000 nm and 1200 nm have been reported.[20,1] Closer inspection of Fig. 2(b) shows that the centers of the absorption band slightly shift towards larger wavelengths and a saturation behavior of the ion-induced maximum k values is observed for increasing fluences approaching $k_{sat} = 0.9$ at about $\lambda = 1400$ nm, which is somewhat higher than typical values obtained electrochemically. The second interesting feature, visible in Fig. 2(a), is the ion-induced ''rotation'' of the real part n of the refractive index around approximately $\lambda^* = 900$ nm with all $n(\lambda)$ values below λ^* being shifted towards smaller and those above λ^* towards larger values. For increasing ion fluences a well-resolved minimum of $n(\lambda)$ is developed at approximately $\lambda = 700$ nm below λ^*, while above, a monotonous enhancement of $n(\lambda)$ is observed up to the highest wavelength of 1600 nm available in the present study. As for the imaginary part, from the sequence of $n(\lambda)$ curves for increasing ion fluences a saturation behavior can be deduced with a maximum value of $n(1600\ \text{nm}) = 2.5$. If the already mentioned ion-induced densification is taken into account, which leads to an additional shift towards higher n values (cf. Fig. 1), the effect of obtaining a fixed $n(\lambda^*)$ becomes even more pronounced as will be demonstrated in the context of He^+ bombardments below [see Fig. 3(a)]. The physics behind this remarkable observation of a fixed point $n(\lambda^*)$, which has also been reported for evaporated WO_3 films colored up to different degrees electrochemically,[21] will be discussed together with the He^+ data.

When ion bombarding sputtered instead of evaporated WO_3 films, qualitatively identical results are obtained, i.e., a

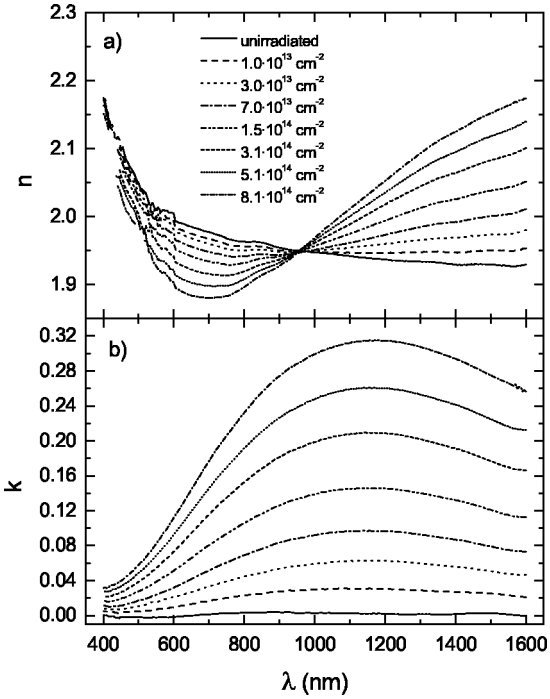

FIG. 3. Dispersion of (a) the real part $n(\lambda)$ and of (b) the imaginary part $k(\lambda)$ for an evaporated WO_3 film (number 17) as changed by 300-keV He^+-ion bombardment with fluences given in the inset.

broad absorption band is induced centered at about 1100 nm and shifting towards 1200 nm for higher ion fluences. Similarly, a fixed point $n(\lambda^*)$ is observed, around which the $n(\lambda)$ values are rotated due to the ion bombardment as described above. In detail, however, it turns out that, within the fluence range employed here, the ion-induced changes neither of $n(\lambda)$ nor of $k(\lambda)$ indicate a saturation behavior. Furthermore, the value of λ^* is slightly shifted to 1200 nm and the maximum value $k_{max}=0.5$ is significantly lower than what can be obtained in evaporated films even with smaller fluences. This latter result points to a less efficient ion-induced coloration in sputtered as opposed to evaporated WO_3 films. To make this observation more quantitative, the maximum value k_{max} for each irradiation step was analyzed as a function of the Ar^+ fluence for evaporated and sputtered films. For the increase of k_{max}, which is signaling the progressing blue coloration as a function of fluence, evaporated films exhibit an approximately ten-times-larger slope $\Delta k_{max}/\Delta\Phi$ than do sputtered ones. If incorporated H_2O can be excluded as the primary source of this difference, the open morphology of evaporated films giving rise to a strongly reduced density may be responsible for this observation. This morphology may cause a very effective removal of oxygen atoms from the interior of a nanograin onto its surface and, from there, even out of the sample, thereby strongly reducing possible recombinations between displaced oxygen and the vacancies both created by the ion bombardment.

Next, the influence of the type of projectile on the ion-induced coloration mechanism was tested by switching to 300-keV He^+. Mostly evaporated WO_3 films were used for these experiments, since they can be colored more effectively by ion bombardment as just mentioned. To allow a direct comparison to the Ar-irradiation data of Fig. 2, the real n and imaginary k parts are again plotted as a function of the wavelength in Fig. 3 for various ion fluences. In this case, the feature already mentioned above of all $n(\lambda)$ curves prepared by He^+-ion bombardment having one common point $n(\lambda^*)$ with $\lambda^*=951$ nm is especially striking. The interpretation of this behavior will be at the focus of the discussion below. Additionally, a comparison of the Ar^+ (Fig. 2) and He^+ (Fig. 3) results immediately shows that within the He-ion fluences applied, neither $n(\lambda)$ nor $k(\lambda)$ exhibit a pronounced saturation behavior leading to an interesting point. If it is assumed that the ion-induced blue coloration is exclusively due to oxygen vacancies created by corresponding displacements during the bombardment, the increase in $k(\lambda)$ should scale with the average number of displacements per atom (dpa), which, in turn, is proportional to the total nuclear energy deposited by a specific projectile in a given target. This latter property can be expressed as ion fluence (Φ) times average nuclear energy loss $(dE/dx)_n$, where the average is taken over the film thickness. It turns out that this nuclear energy loss for 300-keV He^+ ions in WO_3 is approximately smaller by a factor of 330 as compared to 300-keV Ar^+ projectiles.[15] Thus, the maximum He^+ fluence 8×10^{14} cm^{-2} in Fig. 3 corresponds to Ar^+ fluences of the order of 2×10^{12} cm^{-2}, which is the smallest Ar^+ fluence in Fig. 2. This immediately makes clear why no obvious saturation behavior can be yet observed in Fig. 3. There is still another point worth noting. If exclusively ion-induced oxygen displacements are causing the increase in $k(\lambda)$, then, due to its much larger nuclear energy loss, Ar ions are much more efficient for coloration per projectile than He ions. If, however, under the same assumption, the increase in $k(\lambda)$ is plotted versus the average number of displacements calculated as described above, the Ar^+ as well as the He^+ data should collapse onto one curve. Such a collapse, however, is not observed experimentally. While for the Ar bombardment the initial slope of the ion-induced $\Delta k(\lambda=1100\ \text{nm},\Phi)$ per dpa is within the range 7.0 ± 3, for He ions a significantly larger value of 17.0 is obtained. This clearly points to a coloration mechanism in the case of He bombardment additional to oxygen displacements. Consequently, such a mechanism is attributed to the electronic energy loss of the light projectiles. One possibility would be the excitation of electron(e)-hole(h) pairs and their interaction with built-in H_2O according to

$$4e+4h+4W^{VI}O_3+2H_2O\rightarrow4W^{V}O_3+4H^+ +O_2 \quad (2)$$

as suggested in Ref. 9. In this case, the built-in H_2O would act as an internal H^+ source resulting in color centers as in the electrochromic effect.

We now come to the interpretation of the most notable feature of Fig. 3, that all $n(\lambda)$ curves obtained by ion bombardment share a common point $n(\lambda^*)$ with $\lambda^*=951$ nm. The basic idea is to treat the frequency-dependent complex dielectric constant $\varepsilon(\omega)=\varepsilon_1+i\varepsilon_2$, where the real and imaginary parts are related to the complex index of refraction $\tilde{n}=n+ik$ by $\varepsilon_1=n^2-k^2$ and $\varepsilon_2=2nk$, as a superposition of

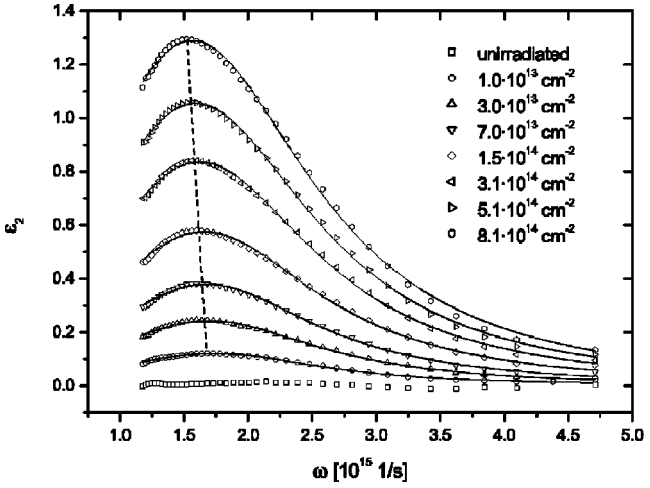

FIG. 4. Frequency dependence of the imaginary part ε_2 of the complex dielectric constant of an evaporated WO_3 film as obtained after 300-keV He^+-ion bombardment with fluences given in the inset. The experimental data points (open symbols) were calculated from $\varepsilon_2 = 2nk$ with n and k taken from Figs. 3(a) and 3(b), while the solid curves represent least-squares fits to ε_{L2} of a Lorentz oscillator as given by Eq. (3).

a contribution $\varepsilon_M(\omega)$ due to the WO_3 matrix and another one due to Lorentzian oscillators $\varepsilon_L(\omega)$ describing the color centers produced by ion bombardment. Furthermore, it is assumed that $\varepsilon_M(\omega)$ remains unaffected by the ion bombardment and, thus, can be calculated from the Cauchy relation $n_M(\lambda)$ fitted to the data of the unirradiated samples together with the approximation $k_M(\lambda)=0$ in this case [cf. Figs. 2(b) and 3(b)]. For the Lorentzian oscillators, on the other hand, the following expressions for the real (ε_{L1}) and imaginary (ε_{L2}) parts were used:

$$\varepsilon_{L1}(\omega) = \frac{A(\omega_0^2-\omega^2)}{(\omega_0^2-\omega^2)^2+\Gamma^2\omega^2},$$

$$\varepsilon_{L2}(\omega) = \frac{A\Gamma\omega}{(\omega_0^2-\omega^2)^2+\Gamma^2\omega^2}. \qquad (3)$$

Here, the parameters ω_0 and Γ determine the frequency position as well as the damping of the oscillators and A includes their density and oscillator strengths. To a first approximation it is expected that ω_0 and Γ as well as the oscillator strength are not or only weakly dependent on the ion fluence, while the density of the ion-induced oscillators should exhibit an exponential saturation behavior for increasing ion fluences reflecting the buildup of color centers created by the bombardment. This simple model of ion-induced identical oscillators is tested by first calculating $\varepsilon_2(\omega,\Phi) = 2n(\omega,\Phi)k(\omega,\Phi)$ for the various ion fluences Φ of the experimental results given in Fig. 3 and then fitting $\varepsilon_{L2}(\omega)$ to these data. The outcome of such an analysis is shown in Fig. 4, where the data $\varepsilon_2(\omega,\Phi)$ are represented by open symbols and the fitting results as solid lines. Clearly, a satisfactory description of the data is obtained by the oscillator model, though it should be noted that all three quantities ω_0, Γ, and A were treated as fitting parameters. Closer inspection of the extracted parameters is delivered in Fig. 5, where Γ as well as ω_0 are plotted versus the ion fluence Φ. While the frequency position ω_0 of the oscillators practically remains constant over the complete series of ion irradiations (observed changes towards smaller values are less than 2%), the damping constants Γ significantly increase as a function of Φ up to an enhancement of about 15%, where they apparently saturate as indicated by the solid line representing an exponential fit to the data. As a consequence of this trend found for Γ, the maxima of $\varepsilon_2(\omega,\Phi)$ in Fig. 4 clearly shift systematically towards lower ω values for increasing fluences (dashed line) as typical for damped oscillators. Furthermore, the observed saturation behavior of $\Gamma(\Phi)$ points to defects created by the bombardment in addition to the ion-induced color centers, which are expected to saturate for increasing fluences and might be able to locally influence the oscillators leading to an overall broadening of the absorption. If, however, for a microscopic description a polaronic picture is used, an alternative interpretation of the observed trends may consist in assuming a growing overlap of polaronic wave functions at higher ion fluences leading to a downshift of the polaron binding energy and hence of the polaronic absorption peak maximum. In this context, it may be worth noting that fitting Gaussians to the data of Fig. 4 results in significantly worse agreement though expected theoretically from a polaron model. More recent theoretical descriptions, however, also are able to give Lorentzians.[22]

As demonstrated in Fig. 6, a similar exponential saturation behavior to for $\Gamma(\Phi)$ is observed for the parameter A (left scale), i.e., $A(\Phi)=\alpha[1-\exp(-\beta\Phi)]$. Fitting this expression to the data (open squares) results in the solid curve and delivers a saturation value $\alpha = 5.4\times10^{-30}\ s^{-2}$ and $\beta = 3.8\times10^{-15}\ cm^2$. The exponential behavior of A is attributed to the creation and final saturation of the density of color centers produced by the ion bombardment. This can be made more quantitative by referring to Smakula's formula,[23]

$$Nf = 0.87\times10^{17}\times[n/(n^2+2)^2]\alpha_{max}W_{1/2}. \qquad (4)$$

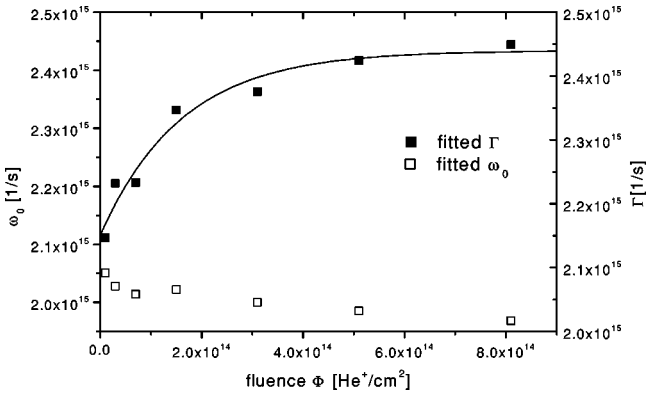

FIG. 5. Lorentz parameters Γ and ω_0 extracted by fitting Eq. (3) to the data of Fig. 4 as a function of the ion fluence Φ. The solid line describes exponential saturation as given by $\Gamma(\Phi)=A[1-\exp(-B\Phi)]+\Gamma_0$ with $A = 2.9\times10^{14}\ s^{-1}$, $B = 6.2\times10^{-15}\ cm^2$, and $\Gamma_0 = 2.1\times10^{15}\ s^{-1}$.

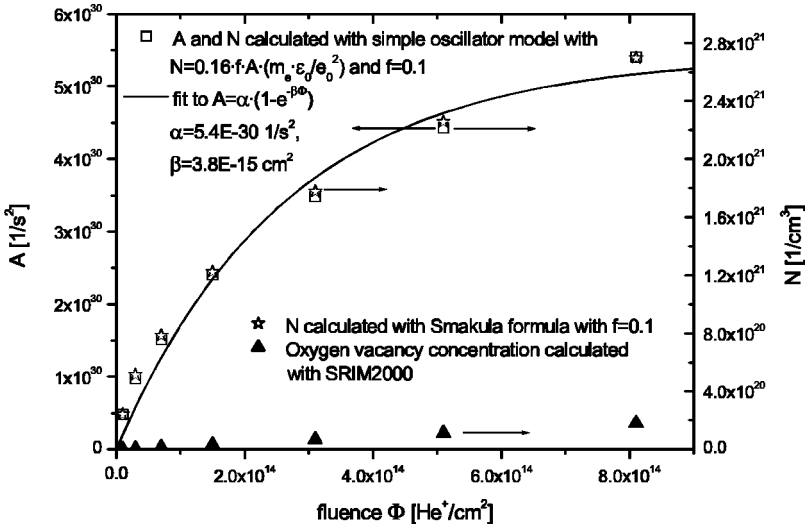

FIG. 6. ''Amplitude'' A (open squares, left scale) of Lorentz oscillators [cf. Eq. (3)] produced by 300 keV He^+ bombardment of an evaporated WO_3 film as extracted from the corresponding fits shown in Fig. 4 versus the ion fluence Φ. The open stars (right scale) represent the ion induced density of color centers N as calculated from the relation given in the inset with a proportionality constant obtained by applying Smakula's fomula (s. text). The closed triangles (right scale) give the density of bombardment induced oxygen vacancies as obtained from Monte Carlo simulations (SRIM).

Here, N is the density of color centers (cm^{-3}), f their oscillator strength, n the refractive index of the as-prepared sample, $\alpha_{max}=2(2\pi/\lambda)k_{max}$ (cm^{-1}) the maximum absorption coefficient with k_{max} being the corresponding maximum of the imaginary part of the bombarded sample, and $W_{1/2}$ (eV) the half width of the absorption band. Using the data of Fig. 3 ($\lambda=1100$ nm, $k_{max}=0.3$, $n=1.95$, $W_{1/2}=1.6$ eV), Eq. (4) gives $Nf=2.7\times10^{20}$ cm^{-3}. Finally, adopting for f the value 0.1,[24] one obtains for the density of He^+-induced color centers $N=2.7\times10^{21}$ cm^{-3}. Since N and A are linearly related, $N=\gamma fA(m_e\varepsilon_0/e_0^2)$ with m_e is the mass, e_0 the charge of an electron, and ε_0 the vacuum dielectric constant, this value has been used to extract the proportionality constant $\gamma=0.16$ allowing to attribute to each A value in Fig. 6 a corresponding density $N(\Phi)$ of the color centers (open stars, right scale in Fig. 6). The maximum value of $N=2.7\times10^{21}$ cm^{-3} induced by the He^+ bombardment is higher than 5×10^{20} cm^{-3} reported for photochromic coloring WO_3 samples,[5,25] while via the electrochromic effect still somewhat higher values, typically 10^{22} cm^{-3}, can be prepared.[24,25] This compares well with the maximum density of ion-induced color centers when using Ar^+. In this case a value of $N=6.5\times10^{21}$ cm^{-3} is obtained, using the data of Fig. 2 ($\lambda=1400$ nm, $k_{max}=0.9$, $n=1.95$) and assuming the same value for $W_{1/2}=1.6$ as above. In this context, still another estimate may be worth noting. Applying Monte Carlo simulations (SRIM2000) of the various ion bombardments of WO_3 films,[16] one can deduce the density of displaced oxygen atoms for each fluence. For the 300-keV He^+ bombardment the corresponding results are included in Fig. 6 as closed triangles. For the highest fluence of $\Phi=8.1\times10^{14}$ cm^{-2} one finds a maximum density of displaced oxygen atoms of approximately 1.8×10^{20} cm^{-3} and possible recombination processes would decrease this density even further. Thus, to obtain the above 2.7×10^{21} cm^{-3}, a mechanism additional to the coloration via displaced oxygen atoms appears to be necessary confirming the idea already given in the context of Fig. 3. On the other hand, in the case of the 300-keV Ar^+ bombardment, SRIM allows an estimate of 1.1×10^{22} cm^{-3} for the density of displaced oxygen atoms for a fluence of $\Phi=1.6\times10^{14}$ cm^{-2}. This is significantly larger than the above given density of 6.5×10^{21} cm^{-3} for the color centers and, thus, clearly points to recombination processes within the much denser cascades produced by the heavier Ar ions.

We now proceed with the analysis of the oscillator model as started with the fitting procedure shown in Fig. 4 for $\varepsilon_{L2}(\omega,\Phi)$. Once the parameters A, ω_0, and Γ are determined for all fluences Φ, the corresponding $\varepsilon_{L1}(\omega,\Phi)$ curves can be calculated according to Eq. (3). On the other hand, from the experimental data of Fig. 3 the real part $\varepsilon_{tot1}(\omega,\Phi)$ can be extracted similarly referring to Eq. (3). Subtracting the oscillator part $\varepsilon_{L1}(\omega,\Phi)$ for each ion fluence Φ from the total real part $\varepsilon_{tot1}(\omega,\Phi)$ should give a series of $\varepsilon_{M1}(\omega,\Phi)$ curves reflecting the behavior of the pure WO_3 matrix. The results are shown in Fig. 7, where $\varepsilon_{tot1}(\omega,\Phi)-\varepsilon_{L1}(\omega,\Phi)$ is plotted as a function of ω. Clearly, for all seven irradiation steps subtraction of the ion-induced oscillator part gives a narrow band of $\varepsilon_{M1}(\omega,\Phi)$ curves including $\varepsilon_{M1}(\omega,\Phi=0)$ representing the unirradiated WO_3 film. One step further, using the fitted Cauchy relation from Fig. 1, which represents an average $n(\lambda)$ behavior for all evaporated as-prepared WO_3 films of this study and assuming $k(\lambda)=0$, an average $\langle\varepsilon_{M1}(\omega)\rangle$ curve can be calculated and the corresponding result is also included in Fig. 7 as a solid line.

The fact that also this averaged $\langle\varepsilon_{M1}(\omega)\rangle$ curve fits within the narrow band demonstrates that an approach is justified of simply adding the effect of ion-induced oscillators to a $\varepsilon_{M1}(\omega)$ curve representing the matrix, which remains practically independent of the bombardment. As a consequence of the above analysis one arrives at the two relations

$$\varepsilon_{tot1}(\omega,\Phi)=\langle\varepsilon_{M1}(\omega)\rangle+\varepsilon_{L1}(\omega,\Phi),$$

$$\varepsilon_{tot2}(\omega,\Phi)=\varepsilon_{L2}(\omega,\Phi). \tag{5}$$

Once $\varepsilon_{tot1,2}(\omega,\Phi)$ is known for each fluence Φ from Eq. (5), the corresponding real part of the refractive index can be calculated from

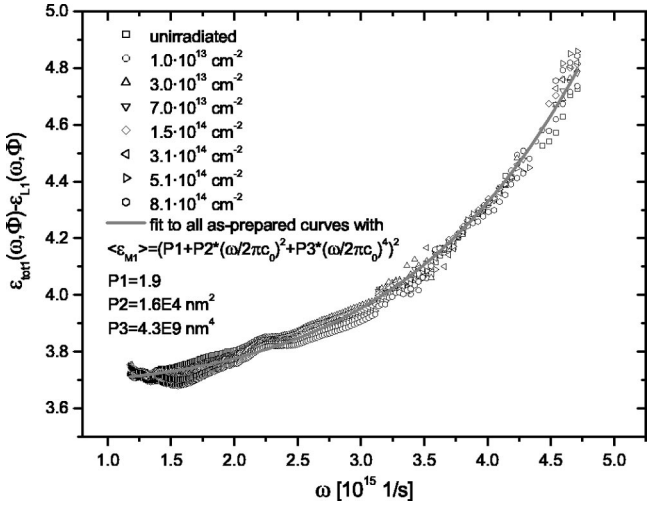

FIG. 7. Difference of the real parts of the experimentally determined dielectric constant and the contribution from the ion-induced Lorentz oscillator as extracted from the fits to Fig. 4 as a function of the angular frequency ω. In our model, this difference represents the WO_3 matrix and should be independent of the ion bombardment. The solid line represents an average WO_3 dispersion $\langle \varepsilon_{M1} \rangle$ obtained from averaging over all evaporated as-prepared WO_3 films (cf. Fig. 1).

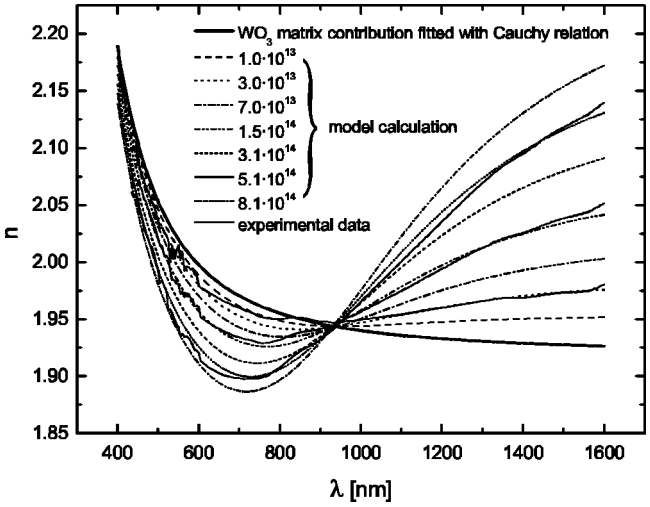

FIG. 8. Dispersion curves $n(\lambda)$ as obtained by modeling the results of the 300-keV He^+-ion bombardment of an evaporated WO_3 film as a superposition of ion-induced Lorentz oscillators and an average matrix contribution, which is independent of the bombardment (details are given in the text). The results of the model calculation correspond to the ion fluences as given in the inset with the thick solid curve representing the average matrix behavior prior to the bombardment. For comparison, the experimental results for the fluences 3.0×10^{13} cm^{-2}, 1.5×10^{14} cm^{-2}, and 5.1×10^{14} cm^{-2} are included as solid curves.

$$n^2(\omega,\Phi)=\frac{\varepsilon_1+\sqrt{\varepsilon_1^2+\varepsilon_2^2}}{2}. \tag{6}$$

The result of this calculation is presented in Fig. 8, here plotted as a function of λ rather than ω to allow a direct comparison to the experimental data $n(\lambda,\Phi)$. This figure clearly demonstrates that the applied model, despite its simplicity, delivers an excellent description of the experimental observations. Especially, what we addressed as the most notable feature of the data, i.e., the existence of a fixed point $n(\lambda^*)$ as described above, is nicely reproduced by the model. In general, if the optical properties of a dielectric are manipulated, e.g., by ion bombardment, in order to observe such a fixed point $n(\lambda^*)$, rather complex interrelated spectral shifts of the real and imaginary parts have to occur imposed by the Kramers-Kronig relations, which make such an observation quite improbable. On the other hand, if the optical properties of a material are dominated by a Lorentz oscillator and different samples just differ by the density of these practically identical oscillators, the Kramers-Kronig conditions are automatically fulfilled and the existence of a fixed $n(\lambda^*)$ is almost trivial with λ^* representing the resonance wavelength of the oscillator. Thus, one can turn the argument around and conclude that the fact of a fixed $n(\lambda^*)$ in the present case of ion bombarded WO_3 films strongly supports the idea of practically identical ion-induced Lorentz oscillators with their density increased by the bombardment, leading to an exponential saturation.

ACKNOWLEDGMENTS

The experimental assistance of R. Durner as well as the financial support by Deutsche Volkswagenstiftung and Deutsche Forschungsgemeinschaft (GK 238 and SFB 569) is gratefully acknowledged.

*Corresponding author. Email address: paul.ziemann@physik.uni-ulm.de; http://www.physik.uni-ulm.de/fkp

[1] Y. Shigesato, Jpn. J. Appl. Phys., Part 1 **30**, 1457 (1991).
[2] O. F. Schirmer, J. Phys. Colloq. **6**, 479 (1980).
[3] C. G. Granqvist, *Handbook of Inorganic Electrochromic Materials* (Elsevier, New York, 1995).
[4] P. M. S. Monk, *Electrochromism, Fundamentals and Applications* (VCH, Weinheim, 1993).
[5] S. K. Deb, Philos. Mag. **27**, 801 (1973).
[6] A. Nakamura and S. Yamada, Appl. Phys. **24**, 55 (1981).
[7] K. Miyake, H. Kaneko, M. Sano, and N. Suedomi, J. Appl. Phys. **55**, 2747 (1984).
[8] M. R. Goulding, C. B. Thomas, and R. J. Hurditch, Solid State Commun. **46**, 451 (1983).
[9] C. Bechinger, G. Oefinger, S. Herminghaus, and P. Leiderer, J. Appl. Phys. **74**, 4527 (1993).
[10] R. A. Dixon, J. J. Williams, D. Morris, J. Rebane, F. H. Jones, R. G. Egdell, and S. W. Downes, Surf. Sci. **399**, 199 (1998).
[11] M. Merz, R. Durner, B. Heinz, and P. Ziemann, Nucl. Instrum. Methods Phys. Res. A **166-167**, 334 (2000).
[12] W. Wagner, F. Rauch, R. Feile, C. Ottermann, and K. Bange, Thin Solid Films **235**, 228 (1993).
[13] R. S. Crandall and B. W. Faughnan, Phys. Rev. Lett. **39**, 232 (1977).
[14] M. Miyakawa, K. I. Kawamura, H. Honsono, and H. Kawazoe, J. Appl. Phys. **84**, 5610 (1998).

[15] B. Heinz, M. Merz, P. Widmayer, and P. Ziemann, J. Appl. Phys. **90**, 4007 (2001).
[16] J. F. Ziegler, J. P. Biersack, and U. Littmark, *The Stopping and Range of Ions in Solids* (Pergamon Press, New York, 1996), Vol. 1.
[17] R. M. Bueno, J. F. Trigo, J. M. Martnez-Duart, E. Elizalde, and J. M. Sanz, J. Vac. Sci. Technol. A **13**, 2378 (1995).
[18] E. Elizalde and F. Rueda, Thin Solid Films **122**, 45 (1984).
[19] F. Abelès and M. L. Thèye, Surf. Sci. **5**, 325 (1966).
[20] Y. G. Mo, R. O. Dillon, and P. G. Snyder, J. Vac. Sci. Technol. A **17**, 2933 (1999).
[21] K. von Rottkay, M. Rubin, and S.-J. Wen, Thin Solid Films **306**, 10 (1997).
[22] P. B. Allen and V. Perebeinos, Phys. Rev. Lett. **83**, 4828 (1999).
[23] A. Smakula, Z. Phys. **59**, 603 (1930).
[24] B. W. Faughnan, R. S. Crandall, and P. M. Heyman, RCA Rev. **36**, 177 (1975). A more recent result, though determined on TiO_2, confirming the value $f=0.1$, is given in S. Eriksen and R.-G. Egdell, Surf. Sci. **180**, 263 (1987).
[25] G. Hollinger, T. M. Duc, and A. Deneuville, Phys. Rev. Lett. **37**, 1564 (1976).